Reversed somatodendritic I_h gradient in a class of rat hippocampal neurons with pyramidal morphology

James B. Bullis[1], Terrance D. Jones[2] and Nicholas P. Poolos[1,2]

[1]*Neurobiology & Behavior and* [2]*Department of Neurology & Regional Epilepsy Center, University of Washington, Seattle, WA 98195-7290, USA*

In CA1 and neocortical pyramidal neurons, I_h is present primarily in the dendrites. We asked if all neurons of a pyramidal morphology have a similar density of I_h. We characterized a novel class of hippocampal neurons with pyramidal morphology found in the stratum radiatum, which we termed the 'pyramidal-like principal' (PLP) neuron. Morphological similarities to pyramidal neurons were verified by filling the neurons with biocytin. PLPs did not stain for markers associated with interneurons, and projected to both the septum and olfactory bulb. By using cell-attached patch-clamp recordings, we found that these neurons expressed a high density of I_h in the soma that declined to a lower density in the dendrites, a pattern that is reversed compared to pyramidal neurons. The voltage-dependent activation and activation time constants of I_h in the PLPs were similar to pyramidal neurons. Whole-cell patch-clamp recordings from the soma and dendrites of PLP neurons showed no significant differences in input resistance and local temporal summation between the two locations. Blockade of I_h by ZD7288 increased the input resistance and temporal summation of simulated EPSPs, as in pyramidal neurons. When NMDA receptors were blocked, temporal summation at the soma of distal synaptic potentials was similar to that seen with current injections at the soma, suggesting a 'normalization' of temporal summation similar to that observed in pyramidal neurons. Thus, we have characterized a principal neuronal subtype in the hippocampus with a similar morphology but reversed I_h somatodendritic gradient to that previously observed in CA1 hippocampal and neocortical pyramidal neurons.

(Resubmitted 29 October 2006; accepted after revision 14 December 2006; first published online 21 December 2006)
Corresponding author N. Poolos: Box 359745, Harborview Medical Center, 325 9th Ave., Seattle, WA 98104, USA.
Email: npoolos@u.washington.edu

Dendrites are the primary location of excitatory synaptic input for most neurons. How synaptic activity is propagated in the dendrites therefore has a profound effect on neural excitability. This propagation is influenced by the passive properties of the dendrites, which shape the amplitude and time course of the postsynaptic response (Rall, 1959, 1962; Segev & London, 2000). The presence of voltage-gated ion channels in the dendrites also influences a neuron's electrotonic properties, and the interaction between ion channels and dendritic morphology is a topic of much research (Johnston *et al.* 1996; Hausser *et al.* 2000; Reyes, 2001; Vetter *et al.* 2001; Hausser & Mel, 2003).

One type of ion channel found in dendrites is the hyperpolarization-activated cation channel (HCN, h-channel), a family of ion channels that is responsible for the current I_h. In CA1 hippocampal pyramidal neurons, I_h is present in a low density at the soma that increases to an over sevenfold higher density in the apical dendrites (Magee, 1998). This pattern is also found in neocortical pyramidal neurons (Berger *et al.* 2001; Williams & Stuart, 2000). Dendritic I_h in CA1 pyramidal neurons has been proposed to normalize temporal summation of EPSPs (Magee, 1999) and reduce the overall neuronal response to excitatory input (Stuart & Spruston, 1998; Poolos *et al.* 2002; Nolan *et al.* 2004). I_h also plays a role in oscillatory firing of thalamocortical relay neurons (McCormick & Pape, 1990), layer II stellate neurons in entorhinal cortex (Dickson *et al.* 2000), and some interneurons of the hippocampus (Maccaferri & McBain, 1996*a*; Lupica *et al.* 2001). In cerebellar Purkinje cells, I_h helps to maintain the resting membrane potential (RMP) in the proper range to maintain high spontaneous firing (Williams *et al.* 2002).

All known pyramidal neurons have a similar gradient of I_h, which suggests it is essential for pyramidal neuron function. We therefore asked if this gradient of I_h is universal to neurons with pyramidal morphology. We characterized a neuron found in the stratum radiatum (SR) of CA1 hippocampus with a pyramidal morphology to test this hypothesis. We have termed these neurons 'pyramidal-like principal' neurons (PLPs). We will show

 DOI: 10.1113/jphysiol.2006.123836

that these neurons, which are probably a subclass of 'radiatum giant cells' (RGC; Gulyas *et al.* 1998), do not stain for interneuronal markers and project to both the septum and olfactory bulb. We found that these neurons have a distinctly different distribution of I_h compared to pyramidal dendrites, with a high density in the soma that declines to a lower density in the apical dendrite. I_h in these neurons had similar biophysical properties to I_h in pyramidal dendrites, and like I_h in pyramidal neurons, modulated temporal summation. PLP neurons therefore violate the correlation between I_h distribution and pyramidal morphology observed in other neurons, and may serve as an additional model with which to test hypotheses regarding dendritic signal integration. Some of these results have been presented previously in abstract form (Bullis *et al.* 2004).

Methods

Electrophysiology

Hippocampal slices (400 μm) were made from 6–10-week-old Sprague-Dawley rats using methods previously described (Poolos *et al.* 2002). Animal protocols were approved by the Institutional Animal Care and Use Committee at the University of Washington. Briefly, rats were anaesthetized with an intraperitoneal injection of a ketamine/xylazine mix (304/19.2 mg kg^{-1}) and perfused intracardially with a modified ACSF, which consisted of (mM): KCl 2.5), NaH_2PO_4 1.25, $NaHCO_3$ 25, $CaCl_2$ 0.5, $MgCl_2$ 7, dextrose 7, choline chloride 110, ascorbate 1.3, and pyruvate 3. All chemicals were obtained from Sigma (St Louis, MO, USA) or Fisher (Houston, TX, USA) unless otherwise stated. Supplemental doses were administered if the animal responded to a foot pinch. The brain was removed and sliced using a Vibratome 1500 sectioning system (St Louis, MO, USA). Slices were kept at 34°C for 10–20 min immediately following slicing, and at room temperature for at least 1 h before recording. Neurons were visualized with infrared differential interference contrast imaging (IR-DIC) using a Zeiss Axioskop (Oberkochen, Germany) fitted with an Olympus objective (Tokyo, Japan). Whole-cell current-clamp recordings were made with a Dagan BVC-700 amplifier (Minneapolis, MN, USA), sampled at 10 KHz, and filtered at 2 KHz. Cell-attached patch recordings were made with an Axon Instruments Axopatch 200B amplifier (Foster City, CA, USA), sampled at 2 KHz, and filtered at 500 Hz. All data were collected and analysed with custom software written for the Igor Pro analysis environment (Wavemetrics; Lake Oswego, OR, USA). Excitatory postsynaptic potentials (EPSPs) were evoked using extracellular stimulation by a constant current pulse (AM Systems Digital Stimulus Isolator; Carlsborg, WA, USA) via a bipolar tungsten electrode. EPSP amplitude was approximately 2–5 mV during recordings. The electrode was placed from 20 to 50 μm from the visualized dendrite along the border of stratum radiatum/stratum lacunosum moleculare.

For recording, slices were kept at 30–32°C and continuously bathed in oxygenated ACSF consisting of (mM): NaCl 125, $NaHCO_3$ 25, dextrose 10, KCl 2.5, $CaCl_2$ 2, $MgCl_2$ 2, and NaH_2PO_4 1.25. Pipettes were made from borosilicate glass and pulled with a Sutter P-87 micropipette puller (Novato, CA, USA). Pipette resistance was between 3–5 MΩ for soma and 4–7 MΩ for dendritic whole-cell recordings. Pipettes were filled with a solution that contained (mM): $KMeSO_4$ 120, KCl 20, Hepes 10, Na_2-ATP 4, $MgCl_2$ 2, Tris-GTP 0.3, EGTA 0.2, pH 7.3 with KOH. For recordings involving synaptic stimulation, 1 mM EGTA was included in the pipette to reduce calcium-related changes in synaptic efficacy during recordings, and 20 μM bicuculline was added to the bath to block inhibitory synaptic input. A cut was made between CA3 and CA1 to minimize spontaneous activity when bicuculline was used. Pipette resistance for cell-attached recordings was between 4–15 MΩ. Pipettes were filled with a solution consisting of (mM): KCl 120, TEA-Cl 20, Hepes 10, 4-aminopyridine 5, $CaCl_2$ 2, $MgCl_2$ 1, $BaCl_2$ 1, pH was adjusted to 7.4 with KOH. For estimations of maximal current density, the area of the patch was obtained from the equation relating patch area to resistance found in Sakmann & Neher (1995), and were elicited at ∼−160 mV. Recordings were accepted only if the resting membrane potential was at least −55 mV and I_h showed rundown of less than 25%. Series resistance for whole-cell recordings was less than 40 MΩ. Group data are expressed as mean ± S.E.M. Unless stated, a one-way ANOVA was used to compare three or more conditions, and an unpaired *t* test for two conditions. Alpha functions were created using the equation:

$$I = I_{max}(\alpha t)(1 - \exp(-\alpha t))$$

where $\alpha = 1.67$. Temporal summation was measured as the fifth EPSP or response divided by the first times 100, which gives the percentage of the response relative to the first event. ZD7288 was obtained from Tocris (Balwin, MO, USA). ZD7288, APV, and bicuculline were made in aqueous stock solutions and bath applied.

Histology

To characterize cellular morphology, pyramidal and PLP neurons were filled via recording micropipettes containing a 0.1–0.3% biocytin (Molecular Probes; Eugene, OR, USA) solution. After recording, slices were fixed overnight with a solution of 4% paraformaldehyde in 0.12 M phosphate buffer. Slices were then blocked overnight in 2% BSA with 0.25% Triton X-100 in 0.03 M PBS,

incubated overnight with streptavidin/Alexa-488 (1 : 200; Molecular Probes) with 0.1% Triton X-100 in PBS, and mounted with Vectashield (Vector Laboratories; Burlingame, CA, USA) on gel-coated slides featuring a custom parafilm (Pechiney Plastic Packaging; Chicago, IL, USA) spacer to allow for sufficient space between the slice and coverslip. Images of the fluorescent neurons were collected in approximately 15 planes through the cells with a Nikon Eclipse TE200/Bio-Rad Radiance 2000 confocal microscope system (El Segundo, CA, USA; Hercules, CA, USA), and processed using Image J software (Wayne Rasband, NIH, USA) into composite projection micrographs. Further anatomical analysis was collected on slices secondarily stained with avidin/horseradish peroxidase (HRP; Vecatastain ABC kit, Vector Laboratories; Burlingame, CA, USA). HRP-treated slices were visualized with a Leica Leitz Laborlux S light microscope (Bannockburn, IL, USA) and photographed using a Nikon Coolpix 4500 digital camera.

Biocytin-filled neurons were examined for colocalization of proteins associated with interneurons, by incubating slices in antibodies for glutamic acid decarboxylase 65/67, calretinin (GAD, CR; Chemicon; Temecula, CA, USA), cholescystokinin-8 (CCK; Immunostar; Hudson, WI, USA), and parvalbumin (PV; Sigma; St. Louis, MO, USA). Fixed and blocked slices were incubated for 24 h in PBS containing 0.3% Triton X-100 and antibodies in concentrations of 1 : 1000 (GAD and CCK) and 1 : 4000 (PV), followed by 1 : 1000 incubation and antirabbit Alexa-568 (GAD and CCK; Molecular Probes; Eugene, OR, USA) and antimouse Alexa-635 (PV; Molecular Probes) for 24 h. These slices were then processed with streptavidin/Alexa-488 as detailed previously. CR immunoreactivity was assayed on fixed hippocampal tissue (without filled neurons) sectioned to 100 μm with a Leica VT 1000 S microtome (Bannockburn, IL, USA). After blocking overnight, slices were incubated for 48 h in 0.05 M TBS with 0.3% Triton X-100 containing antibodies for CR raised in the goat (1 : 8000, Chemicon), followed by incubation in antigoat Alexa-568 (1 : 1000).

To determine immunoreactivity for proteins associated with excitatory neurons, fixed tissue was sectioned to 100 μm, incubated with goat antibodies for excitatory amino acid transporter 3 (EAAT3, EAAC1; 1 : 4000; Chemicon) in TBS (containing no Triton X-100) for 48 h, and finally incubated with antigoat Alexa-568 (1 : 1000) in TBS for 24 h. All incubations and washes were performed at 4°C, and slices were mounted and imaged as described above.

Retrograde labelling of PLP neuronal projections

Injections of the retrograde tracer cholera toxin conjugated with Alexa-488 (CTB; Molecular Probes) were made into the olfactory bulb and lateral septum of animals anaesthetized with 4–5% isofurane, to examine the axonal projections of PLP neurons. Using a Hamilton syringe, 2 μl of CTB were administered in the olfactory bulb at three stereotaxic positions previously used by Gulyas *et al.* (1998) (AP: 9, L: 1.3; D: −3.5; AP: 8, L: 1.1 D: −2.5; AP: 6.5, L: 1.1 D: −1.5 from bregma). Septal injections of 3 μl CTB were made at coordinates AP: 0.7, L: 0.7 D: 6.0 from bregma (Paxinos & Watson, 1998). The animals recovered from surgery for three days, allowing for tracer uptake by axon terminals and retrograde transport. Following recovery, animals were anaesthetized by a similar method to the electrophysiology experiments and intracardially perfused with PBS and 4% paraformaldehyde. Harvested brain tissue was then sectioned to 100 μm, washed in PBS (3 × 60 min), and visualized with fluorescent confocal microscopy.

Results

PLP morphology

We identified a class of neurons in the hippocampus with pyramidal morphology to test whether they had a similar distribution of I_h as pyramidal neurons. We have termed these neurons 'pyramidal-like principal' (PLP) neurons, based on our characterization below. We chose these neurons in part because they are easily located in the stratum radiatum (SR) using infrared differential interference contrast microscopy (IR-DIC). Their relative isolation allowed for both easier patch clamping at the soma and tracing of their dendrites for dendritic recordings. Figure 1*A* shows typical IR-DIC micrographs of both pyramidal and PLP neurons. The soma of the PLP is isolated, while the pyramidal neurons are surrounded by other somata in the stratum pyramidale (SP).

PLP somata in CA1 SR were normally located 25–100 μm distal from the SP. They were found throughout CA1, but in higher densities closer to the subiculum. While also present in CA3, we did not further characterize these neurons. The pyramidal-shaped somata of PLPs were usually 5–10 μm larger than pyramidal neurons both in width and height, with a prominent apical dendrite extending to the stratum lacunosum moleculare (SLM). There was a low density of PLP neurons relative to pyramidal neurons. A typical 400 μm slice would contain from five to ten PLPs in CA1, while hundreds of pyramidal neurons would be present.

Fluorescent staining of a biocytin-filled CA1 pyramidal neuron (Fig. 1*B*) and PLP neuron (Fig. 1*C*) revealed a cylindrical or biconical radiation of dendrites common to pyramidal neurons (Fiala & Harris, 1999). The proximal apical dendrites of both types of neurons typically had oblique branches that did not branch extensively. The apical dendrites of both neuron types would often bifurcate

after a minimum of 50 μm into branches that themselves branched into many terminal processes. Both neuron types also showed basal dendrites, with several smaller processes emanating from the soma that did not extensively branch. Location, branching, and the projection of PLP dendrites were confirmed with light microscopy and horseradish peroxidase staining of a biocytin-filled PLP neuron in Fig. 1*D*, which shows a PLP soma located approximately 50 μm from the SP, and demonstrates the extension of the apical dendrite into the SLM. The axons of some PLP neurons were visible projecting to the alveus (Fig. 1*C*, *E* and *F*; arrowheads), while others also bifurcated (Fig. 1*E*), which suggested that PLP neuron axons project both outside of the hippocampus and to the subiculum and entorhinal cortex, although subicular and entorhinal connections were not verified. In two cases where spines were apparently visible in low-resolution images, higher-resolution images confirmed the presence of spines on secondary dendritic branches (Fig. 1*G*; arrowheads). These results indicate that PLP and pyramidal neurons share a similar dendritic morphology.

PLPs lack inhibitory interneuronal markers

The presence of spines on the dendrites of PLPs combined with the projection of their axons to the alveus suggested that PLPs are excitatory neurons (but see Hsu & Buzsaki, 1993). We sought to determine if PLPs were excitatory or inhibitory by staining for typical interneuronal markers glutamic acid decarboxylase 65/67 (GAD), parvalbumin (PV), cholescystokinin-8 (CCK), and calretinin (CR;

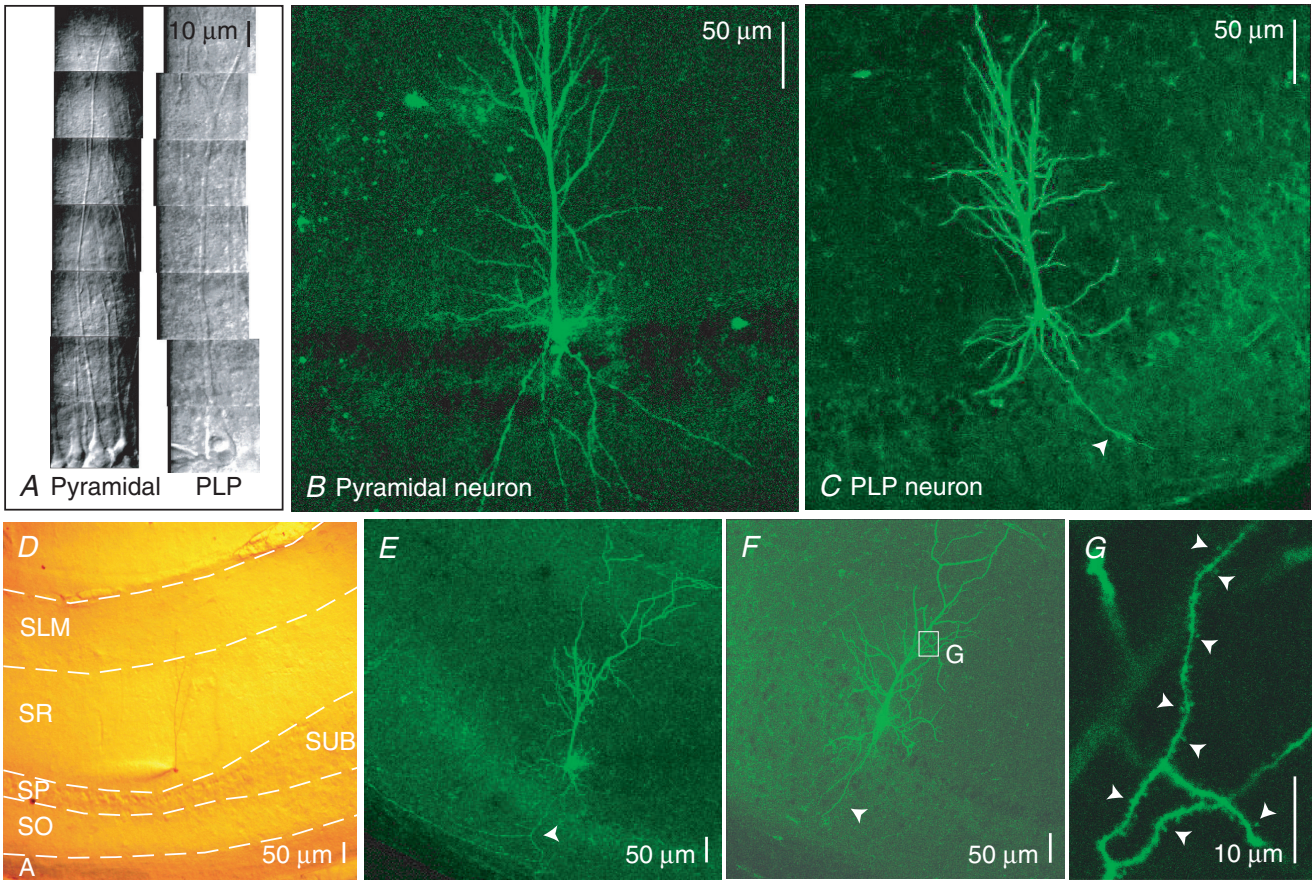

Figure 1. PLP neuron morphology is similar to that of pyramidal neurons
A, a pyramidal-shaped soma and prominent apical dendrites are common to both CA1 hippocampal pyramidal and PLP neurons, as seen in IR-DIC microscopy. *B* and *C*, composite projection images of biocytin-filled CA1 pyramidal and PLP neurons stained with streptavidin/Alexa-488 showed similar branching of apical, oblique, and basal dendrites. The axon was visible projecting to the alveus (arrowhead). *D*, typical PLP location was exemplified with a biocytin-filled PLP neuron (same neuron as *C*) resolved with horseradish peroxidase. The PLP soma was within the proximal stratum radiatum (SR), while the apical dendrite extended to the stratum lacunosum-moleculare (SLM). *E* and *F*, PLP neurons showed typical pyramidal morphology and axons extending to the alveus (arrowheads). In *E*, the axon was also observed to bifurcate in the stratum oriens. *G*, magnification of the secondary dendrites of the PLP neuron from *F* revealed numerous spines (arrowheads).

Freund & Buzsaki, 1996, McBain & Fisahn, 2001). When biocytin-filled neurons were counterstained for these markers, PLPs were found to be immunonegative for GAD, PV, CCK, and CR (Fig. 2*A* and *B*; CCK data not shown), while neurons that matched morphological descriptions of previously described interneurons were clearly visible (Freund & Buzsaki, 1996; McBain & Fisahn, 2001). In Fig. 2*A*, numerous neurons were present that stained for GAD. Antibodies for PV primarily stained neurons with somata located in the SP, with some apical processes visible in the SR consistent with the known location of PV-positive basket cells and chandelier cells (Freund & Buzsaki, 1996). In Fig. 2*B* the dendritic morphology of neurons stained for CR was multipolar, with little branching, while neurons of a pyramidal morphology were not stained. This branching is consistent with the description of CR interneurons as having bipolar dendrites (Freund & Buzsaki, 1996; Gulyas *et al.* 1996).

We then incubated slices with an antibody for excitatory amino acid transporter 3 (EAAT3, EAAC1). Although known to be present on inhibitory neurons in the cerebellum, EAAT3 consistently stains pyramidal neurons in the hippocampus (Rothstein *et al.* 1994; Kanai *et al.* 1995). We found dense staining for both pyramidal neurons and neurons with PLP morphology in the SR (Fig. 2*C*, arrowhead). Also present were neurons with the typical 'radiatum giant cell' (RGC) morphology (Gulyas *et al.* 1998) as described below (Fig. 2*C*, arrow). The observed staining for markers found predominantly in excitatory neurons, and lack of staining for inhibitory neuron markers suggested that PLP neurons were excitatory.

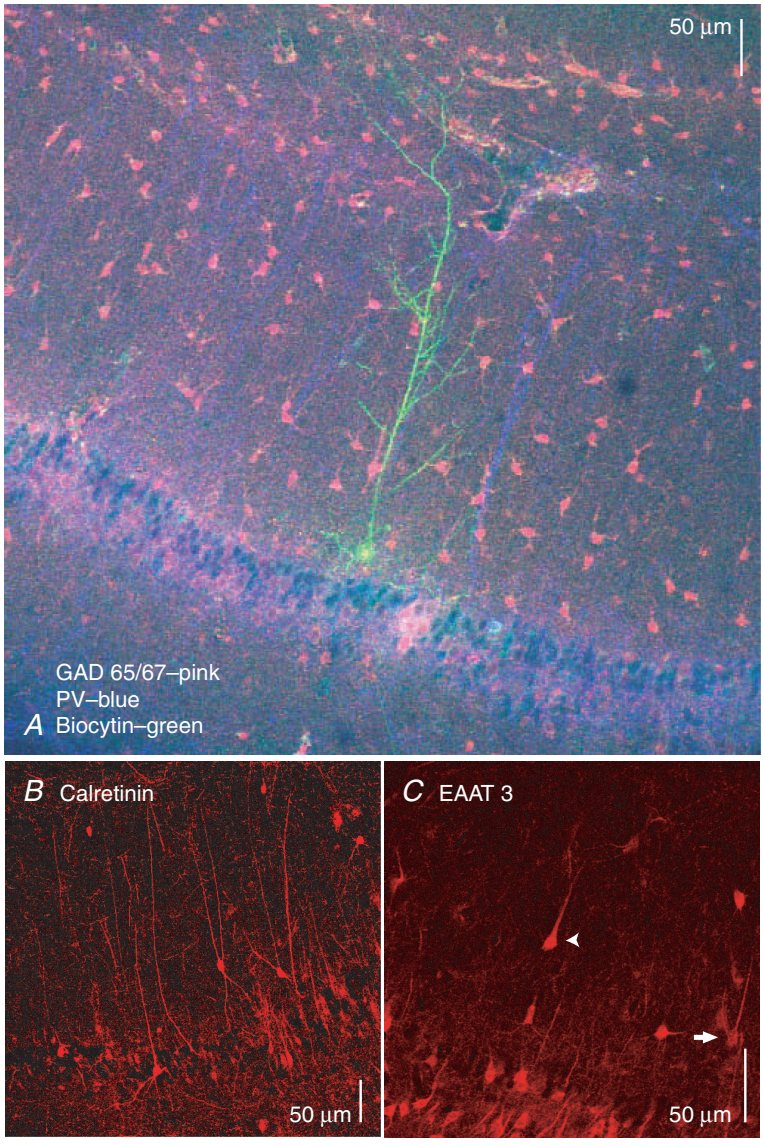

Figure 2. PLP neurons do not stain for interneuronal markers
A, PLPs were immunonegative for glutamic acid decarboxylase 65/67 (GAD 65/67; pink) and parvalbumin (PV; blue). GAD-positive interneurons were visible in all layers of CA1, in addition to the PV-positive dendrites of putative basket cells (blue). A biocytin-filled PLP neuron was stained with streptavidin/Alexa-488 (green). *B*, calretinin-positive interneurons were brightly stained, while neurons with PLP morphology were not visible. *C*, staining for excitatory amino acid transporter 3 (EAAT3) revealed an immunopositive PLP neuron (arrowhead) and a radiatum giant cell (RGC; arrow), along with numerous pyramidal neurons.

PLPs project to subcortical regions

It is known that CA1 hippocampal pyramidal neurons project to the septum and olfactory bulb while also projecting within the hippocampal formation to the subiculum and entorhinal cortex in rats (van Groen & Wyss, 1990). Interneurons of the hippocampus, however, project only locally (Freund & Buzsaki, 1996; McBain & Fisahn, 2001). We therefore sought to test whether PLPs have similar projections as CA1 pyramidal neurons by injecting the retrograde tracer cholera toxin Alexa-488 (CTB) into the septum. After three days we examined hippocampal slices to find dense staining of pyramidal neurons and neurons with PLP morphology in the SR (Fig. 3*A*; arrowhead). We also found neurons with two prominent apical dendrites, which is typical for RGCs and consistent with prior reports of their projection outside the hippocampus (Gulyas *et al.* 1998; Fig. 3*B*, arrow). We then administered CTB into the olfactory bulb and again found staining of neurons with PLP morphology in the SR (Fig. 3*C* and *D*). Olfactory injections only intermittently labelled pyramidal neurons, which is similar to what was observed in earlier retrograde staining (van Groen & Wyss, 1990; Gulyas *et al.* 1998). Together, these data suggest that PLPs are a principal neuron of the hippocampus.

One distinction between PLPs and pyramidal neurons is apparent in the scarcity of pyramidal neuron projections to the olfactory bulb. This pattern of projection is similar to the RGC, a class of principal neurons in the hippocampus (Gulyas *et al.* 1998; Christie *et al.* 2000; Kirson & Yaari, 2000; Savic & Sciancalepore, 2001). RGCs also project to the olfactory bulb, and make asymmetrical synapses with other neurons (Gulyas *et al.* 1998). Most RGCs also have two prominent apical dendrites that project to the SR/SLM. The somata of these neurons normally have the shape of an inverted triangle, and have little basal branching (Gulyas *et al.* 1998; Kirson & Yaari, 2000). A minority of RGCs have been described with a more typical pyramidal appearance, particularly the 'P-cell-like' class described by Gulyas *et al.* (1998) Although PLPs are probably a subclass of

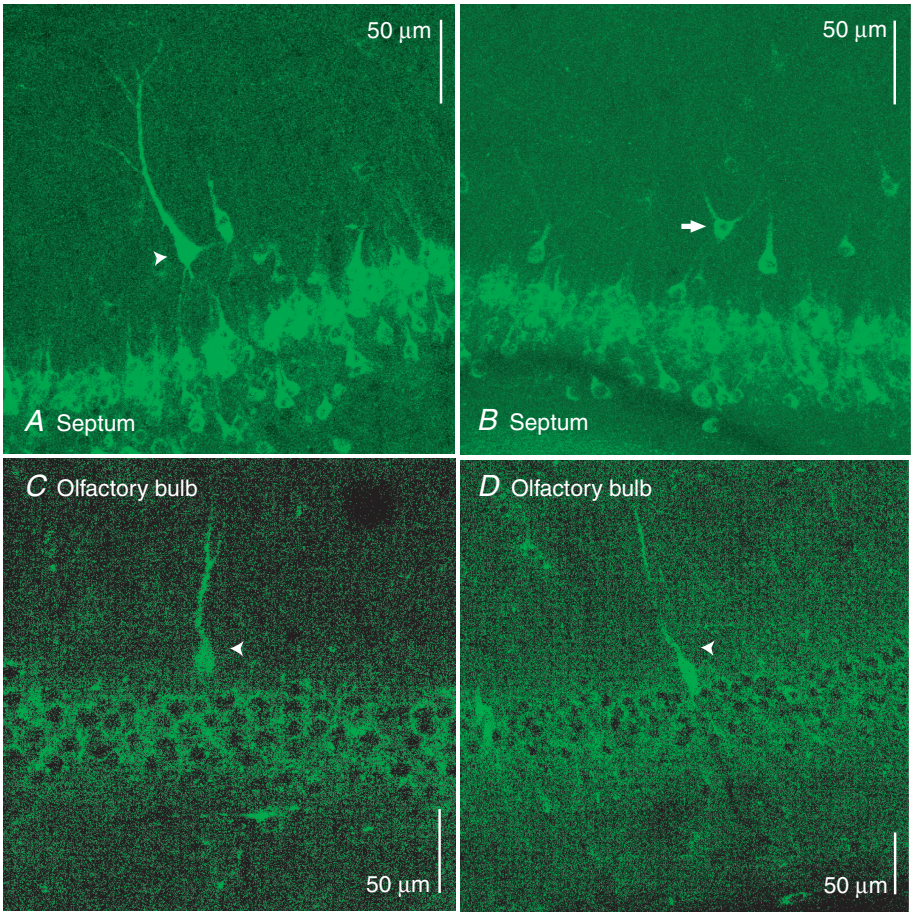

Figure 3. PLP neurons project to the septum and olfactory bulb
A, a PLP neuron (arrowhead) was labelled with the retrograde tracer cholera toxin (CTB) conjugated with Alexa-488 three days after the tracer was injected into the septum. *B*, septal injection also labelled a radiatum giant cell (arrow) as well as pyramidal neurons. *C* and *D*, PLPs stained (arrowheads) from CTB injected into the olfactory bulb three days post-injection. Pyramidal neurons showed little or no staining.

RGCs, we chose a distinct nomenclature to emphasize the significantly different morphology of the PLP compared to the typical non-pyramidal RGC morphology.

In summary, we found similarities in morphology between PLP and pyramidal neurons based upon visualization of biocytin-filled neurons. PLPs do not stain for interneuronal markers, but do stain for an excitatory marker, which suggests that PLP neurons are excitatory. Finally, we found that PLP and pyramidal neurons project to the septum and olfactory bulb, although to differing extents.

PLPs have a gradient of I_h density that is reversed from that in CA1 pyramidal neurons

I_h in CA1 pyramidal neurons is known to be present in a gradient pattern, with a low density in the soma that increases sevenfold in the apical dendrites (Magee, 1998). We sought to determine if the PLP neuron had a similar gradient of I_h using cell-attached patch recordings. Figure 4*A* shows typical current traces from PLP soma and dendrite recordings. Unlike CA1 pyramidal neurons, PLP somata had higher maximal currents than in PLP dendrites. We measured I_h at dendritic distances up to 180 μm from the PLP soma. Because of the location within the SR and larger size of PLP somata, this distance was at or beyond the SR–SLM border, and thus represented distal recording sites for PLP neurons. By normalizing for patch area (Sakmann & Neher, 1995), we found an average density of 14 ± 1.5 pA μm^{-2} in the PLP somata ($n = 20$). The average density in the first 60 μm of the dendrites was 7.8 ± 1.9 pA μm^{-2} ($n = 18$). For the second 60 μm, the density was 6.4 ± 1.0 pA μm^{-2} ($n = 10$) and for the final 60 μm the density was 5.3 ± 1.3 pA μm^{-2} ($n = 6$; Fig. 4*B*). Maximal I_h density was significantly lower in the dendrites compared to the soma ($P < 0.05$; Kruskal–Wallis ANOVA). Although the means declined through the dendritic compartments, differences between

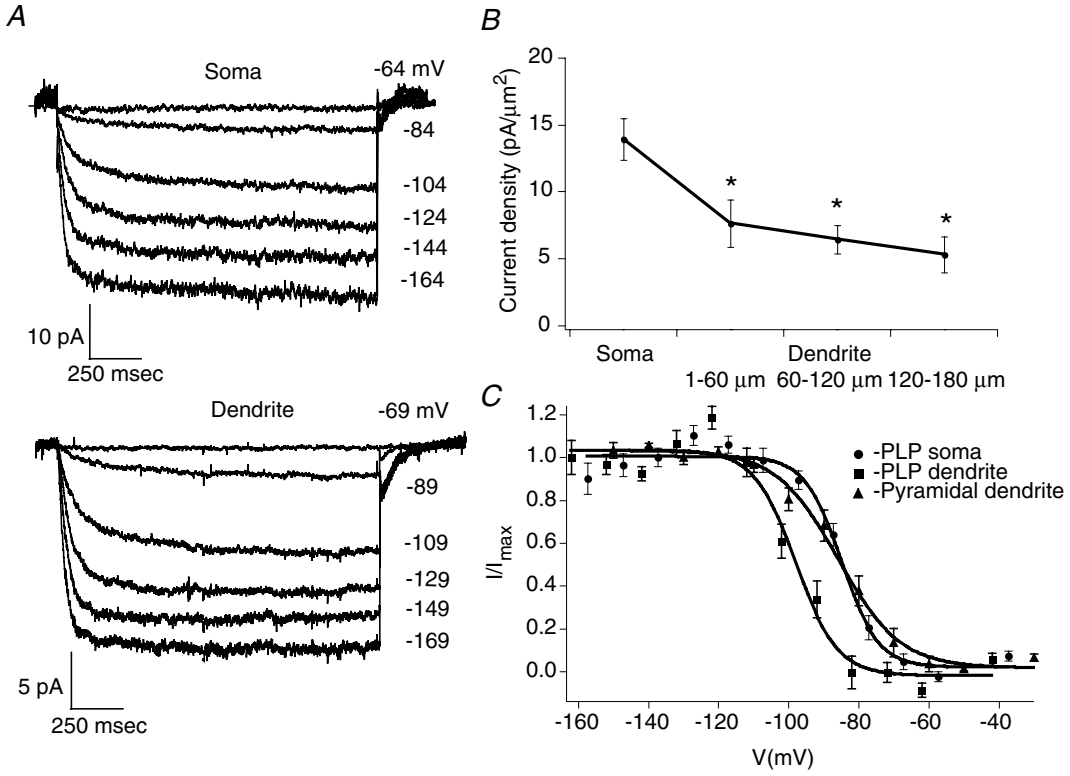

Figure 4. PLP neurons have a high density of I_h in the soma and a declining density in the dendrites
A, I_h traces from cell-attached voltage-clamp recordings from the soma and the dendrites of two separate PLP neurons are shown. PLP soma traces had a maximal current approximately two times that of the PLP dendrite, which was recorded 113 μm from the soma. Numbers on the right of the traces represent the voltage command. *B*, binned PLP current density *versus* somatodendritic distance was measured from an ~ -160 mV step and normalized for patch area. PLP I_h showed a declining density from the soma to the distal dendrites (*$P < 0.01$ compared to soma, Kruskal–Wallis ANOVA). *C*, voltage-dependent activation curves were plotted from PLP somata (●), PLP dendrites recorded at an average distance of 106 ± 9.3 μm (■), and pyramidal neuron dendrites (▲) recorded at an average distance of 156 ± 7.5 μm. PLP somata showed a similar activation curve to pyramidal dendrites, while PLP dendrites had a hyperpolarized shift of approximately 10 mV.

these compartments were not significant. The density of I_h in PLP somata was similar to what we found in the apical dendrites of pyramidal neurons (12 ± 3.4 pA μm^{-2}; $n = 12$) at a mean distance of $156\ \mu m \pm 7.5\ \mu m$ ($n = 12$) with a mean patch area of $2.8 \pm 0.13\ \mu m^2$ ($n = 11$).

Biophysical characteristics of I_h are similar between PLP somata and pyramidal dendrites

We measured the biophysical properties of I_h observed in PLP soma and dendrite recordings from the furthest two bins (range between 60 and 180 μm; average $106 \pm 9.3\ \mu m$), and compared them to those in CA1 pyramidal dendrites. Voltage-dependent activation was found by measuring the normalized tail currents and fitting the current–voltage relationship with a Boltzmann function (Fig. 4*C*). We found a mean half-activation voltage ($V_{1/2}$) of -84 ± 3.0 mV for PLP somata ($n = 11$), -95 ± 2.4 for PLP dendrites ($n = 10$), and -86 ± 3.4 mV ($n = 7$) for pyramidal dendrites. The $V_{1/2}$ was significantly hyperpolarized for PLP dendrites compared to PLP somata or pyramidal dendrites ($P < 0.05$), but was not significantly different between pyramidal dendrites and PLP somata. A similar trend in $V_{1/2}$ across the somatodendritic axis has also been observed in pyramidal neurons (Magee, 1998).

Activation time constants were measured by fitting the current evoked near $V_{1/2}$ with a double-exponential function. I_h shows a double-exponential time course in CA1 pyramidal neurons, reflecting the expression of both HCN1 and HCN2, with HCN1 activation normally an order of magnitude faster than HCN2 (Santoro *et al.* 2000; Chen *et al.* 2001; Ulens & Tytgat, 2001; Robinson & Siegelbaum, 2003). Slow activation time constants were 624 ± 94.8 ms for PLP somata ($n = 11$), 740 ± 189 ms for PLP dendrites ($n = 10$), and 660 ± 179 ms for pyramidal dendrites ($n = 7$). There were no significant differences between groups. Fast activation time constants were 79 ± 10 ms for PLP somata, 75 ± 11 ms for PLP dendrites, and 54 ± 8.7 ms for pyramidal dendrites. Again, the groups did not significantly differ. The similarities of both voltage-dependent activation and time constants demonstrate that I_h is equivalent in pyramidal and PLP neurons, thus both neurons probably have a similar composition of HCN1 and HCN2 subunits.

Following cell-attached patch recording, we ruptured the patch to determine the resting membrane potential (RMP). I_h is known to depolarize the RMP, which in some interneurons of the hippocampus influences their spontaneous firing (Maccaferri & McBain, 1996*a*; Lupica *et al.* 2001). PLP somata had a RMP of -67 ± 1.7 mV ($n = 11$), while PLP dendrites had a RMP of -72 ± 2.8 mV ($n = 11$), with no significant difference between the two locations ($P > 0.05$). The RMP of pyramidal dendrites was -60 ± 1.3 mV ($n = 7$), which was significantly depolarized compared to the RMP of PLP somata and dendrites ($P < 0.05$). This could reflect the reduced I_h in PLP dendrites relative to pyramidal dendrites, which would cause a hyperpolarizing shift in the RMP, although other ion channels also help set the RMP in neurons (Day *et al.* 2005).

I_h contributes to PLP intrinsic properties

Whole-cell current-clamp recordings were performed at the soma and dendrites to characterize the influence of I_h on the intrinsic properties of PLP neurons. Dendritic recordings were made at a range of 125–175 μm, with an average of $142 \pm 6.1\ \mu m$ ($n = 10$). Because K-gluconate blocks I_h and some K^+ currents (Velumian *et al.* 1997), we used $KMeSO_4$ in our internal solution to measure the passive properties of PLP neurons. By giving depolarizing current steps in 100 pA increments for 600 ms, we found marked accommodation of action potential (AP) firing in most PLP neurons (Fig. 5*A*), similar to that in CA1 hippocampal pyramidal neurons. Most of the neurons examined clearly showed a spike after-depolarization (Fig. 5*A*, arrowhead), which is common in pyramidal and RGC neurons (Gulyas *et al.* 1998). Hyperpolarizing current injections in all neurons produced a sag in steady-state membrane potential, indicating I_h activation (Fig. 5*A*; arrow).

We used similar methods when recording from the dendrites of PLP neurons. Depolarizing current steps given to PLP dendrites produced initial APs of smaller amplitudes than somatic APs, with decrementing amplitudes of subsequent APs. Figure 5*B* shows an example from a dendritic recording made at 150 μm. Pyramidal neuronal dendrites in CA1 also show a similar spiking behaviour (Stuart & Sakmann, 1994; Colbert *et al.* 1997; Jung *et al.* 1997), thus it appears that PLP dendrites support back-propagating action potentials. Hyperpolarizing current steps produced the 'sag' also observed in the soma, indicating the presence of h-channel activity.

We sought to verify the contribution of I_h to PLP passive membrane properties by bath-applying ZD7288 (20 μM), a membrane-permeable and specific inhibitor of I_h (Harris & Constanti, 1995), during somatic recordings (Fig. 5*C*). To control for variability in the RMP, we held the membrane potential at -65 mV. Current injections in the presence of ZD7288 after 30 min produced a greater voltage response than in control conditions, and were sufficient to invoke firing in response to a previously subthreshold current injection. The voltage sag indicative of I_h was also reduced in the presence of ZD7288.

We measured the steady-state input resistance (R_{in}) in response to 100–300 pA hyperpolarizing current

injections (Fig. 5*D*) and found a R_{in} of 56 ± 2.8 MΩ for PLPs ($n = 25$) recorded under control conditions in the soma, and 51 ± 4.9 in the dendrites ($n = 10$). There was no significant difference between input resistance at the soma and the dendrites. After 30 min of incubation, ZD7288 significantly increased R_{in} at the soma to 144 ± 8.5 MΩ ($n = 14$) as expected, indicating a significant contribution of I_h to the input resistance ($P < 0.001$).

Blockade of I_h by ZD7288 also hyperpolarized the RMP of PLP neurons. The RMP in PLPs hyperpolarized from -66 ± 0.9 to -72 ± 1.0 ($n = 16$) following application of ZD7288 ($P < 0.001$, paired t test). I_h thus helps to set the RMP of PLP neurons, although other ion channels are probably involved as well (Day *et al.* 2005).

I_h in PLPs alters temporal summation similarly to pyramidal neurons

I_h plays a role in temporal summation (TS) of pyramidal neurons (Magee, 1999; Poolos *et al.* 2002). This effect is most prominent at a frequency of 20 Hz, and less at other frequencies. To see if the same effects are observed in PLP neurons, we measured the response of PLP neurons to alpha-function current injections at different frequencies to simulate EPSPs. We used a train of five alpha functions at 10 Hz, 20 Hz, and 40 Hz delivered to the soma or dendrites of PLP neurons. Representative voltage responses of a neuron to trains of alpha functions are shown in control conditions and following application of ZD7288 (20 μm; Fig. 5*E*). Following application of

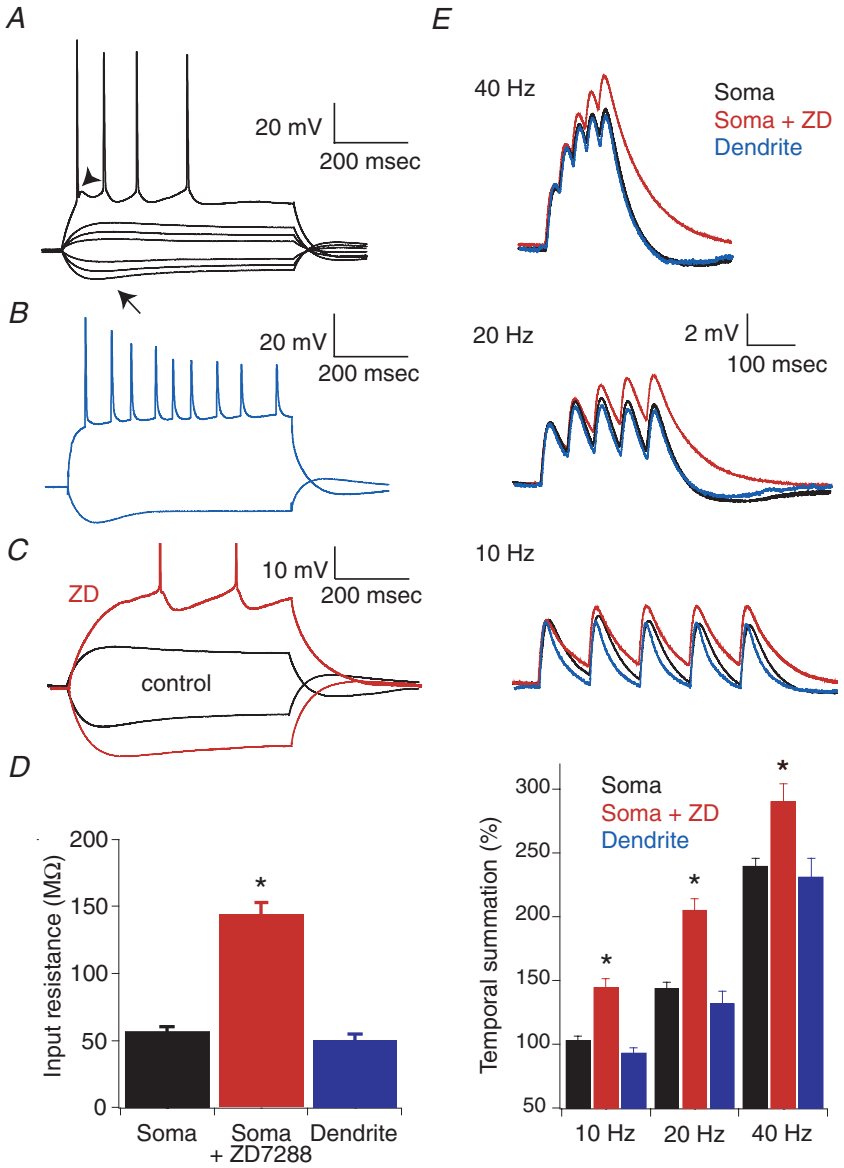

Figure 5. Intrinsic properties of PLP neurons
A, voltage response of a PLP neuron showed the 'sag' (arrow) elicited by hyperpolarizing current steps, indicating the presence of I_h. For a 700 pA depolarizing current step, the neuron fired with rapid accommodation. The afterdepolarization is visible following the first action potential (arrowhead). *B*, dendritic recording from a PLP neuron (recorded at 150 μm) in response to a 500 pA depolarizing and a 300 pA hyperpolarizing current injection showed decremental back-propagating action potential firing. *C*, the response of the neuron in (*A*) to a depolarizing and hyperpolarizing 200 pA current step shown under control conditions (black traces) and in the presence of ZD7288 (red traces; 20 μM). The neuron showed a markedly greater voltage deflection with blockade of I_h. *D*, the mean input resistance (R_{in}) of PLP soma in control conditions (black) significantly increased in the presence of ZD7288 (red; 20 μM; $^*P < 0.01$; paired t test). R_{in} from PLP dendrites under control conditions (blue) was not significantly different from PLP somata. *E*, recordings from the PLP som in (*A*) in response to five alpha function current injections delivered at 10, 20, and 40 Hz under control conditions (black traces) and after exposure to ZD7288 (20 μM; red traces). A PLP dendrite recorded under control conditions at 175 μm (blue) showed similar TS as at the soma. All responses have been normalized to the first alpha injection from PLP soma controls. TS was measured as the percentage of the neuron's response to the fifth alpha injection relative to the first. Pooled data showed that TS was increased by blockade of I_h with ZD7288 at the soma ($^*P < 0.01$, paired t test), but was similar under control conditions between the soma and dendrites.

ZD7288, there is a visible increase in the amplitude and time course of the neuronal response to the alpha current injection, leading to an overall increase in TS across frequencies. TS (Fig. 5*E*) in control conditions was: 103 ± 3.1%, 143 ± 4.5%, and 238 ± 5.4% ($n = 19$) for 10, 20, and 40 Hz, respectively. Following ZD7288 treatment, TS was: 145 ± 6.8%, 205 ± 9.4%, and 290 ± 14% ($n = 10$) for 10, 20, and 40 Hz, respectively. For dendrites in control conditions TS was: 93 ± 4.0%, 131 ± 9.8%, and 231 ± 14.5% ($n = 10$) for 10, 20, and 40 Hz, respectively. For all frequencies, ZD7288 significantly increased TS ($P < 0.01$, paired t test), but no difference between soma and dendrites was detected. In summary, I_h in PLP neurons decreased temporal summation, with the greatest change coming at 20 Hz, the frequency most sensitive to I_h blockade in pyramidal neurons. Local summation, however, was constant from soma to dendrites.

PLP input is normalized across the somatodendritic axis

To further clarify the role of temporal summation in PLP neurons, we evoked excitatory postsynaptic potentials (EPSPs) in PLP neurons by extracellularly stimulating afferents along the border of the SR–SLM (Fig. 6*A*). We measured the amount of EPSP summation in the neurons to five stimuli delivered at 10, 20, and 40 Hz, and blocked I_h by ZD7288 (20 μm) to isolate its effects on TS. TS was: 141 ± 6.7%, 263 ± 18.4%, and 455 ± 31.7% for 10, 20, and 40 Hz, respectively, under control conditions ($n = 4$). Following application of ZD7288, TS increased to: 238 ± 22%, 339 ± 4.1%, and 544 ± 52% for 10, 20, and 40 Hz, respectively, a significant increase for 10 and 20 Hz ($P < 0.05$, paired t test). These results are higher than TS measured with current injections, and suggest

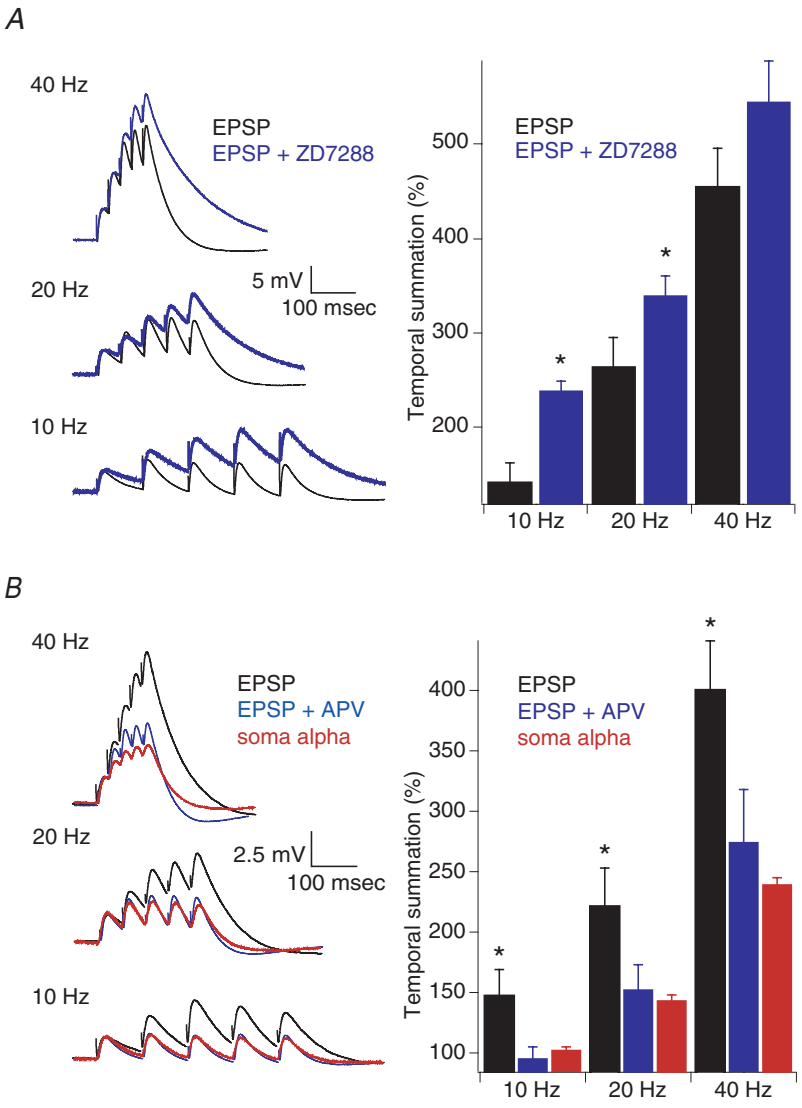

Figure 6. Synaptic properties of PLP neurons
A, EPSPs recorded at the soma elicited by stimulation at the border of the SR–SLM at frequencies of 10, 20, and 40 Hz, are shown under control conditions (black) or in the presence of ZD7288 (20 μM; blue). Blockade of I_h caused a significant increase in TS at 10 and 20 Hz (*$P < 0.05$, paired t test) compared to controls. *B*, EPSPs were generated similarly to *A* under control conditions (black) and with blockade of NMDA receptors by APV (100 μM; blue). The response to alpha function current injections at the soma of the neuron in Fig. 5*B* are also displayed (red). Under control conditions, synaptic stimulation produced markedly increased TS, which was NMDA receptor-dependent. Pooled data for EPSP temporal summation were measured similarly to Fig. 5*B*. In the presence of APV, synaptic stimulation showed a significant decrease in TS (*$P < 0.05$) compared to control, and was similar to that seen with alpha current injections at the soma.

that synaptic events may be a critical factor in TS beyond the intrinsic properties of the neuron.

A potentially important component to EPSP summation is activation of NMDA receptors, particularly for RGCs, which may have a unique NMDA component to their EPSPs (Kirson & Yaari, 2000). We blocked NMDA receptors with DL-2-amino-5-phosphopentanoate (APV; 100 μM) and found a significant reduction in EPSP summation (Fig. 6*B*). Prior to infusion of APV, TS was: $146 \pm 21.5\%$, $222 \pm 32.2\%$, and $400 \pm 41.1\%$ ($n = 6$, $P < 0.05$) for 10, 20, and 40 Hz, respectively. APV reduced TS to $96 \pm 10.3\%$, $152 \pm 20.9\%$, and $274 \pm 44.1\%$ ($n = 6$). Interestingly, when NMDA receptors were blocked, TS was similar to values observed from alpha current injections at the soma. Comparisons of TS reveal significant differences between EPSPs in control conditions and following infusion of APV ($P < 0.05$), but no difference between EPSPs in APV and alpha current injections at the soma. This would suggest that TS is 'normalized' in PLP neurons as it is in pyramidal neurons (Magee, 1999).

These results show that PLP neurons have I_h that is similar in biophysical properties to that of pyramidal neurons, but found in a reversed somatodendritic gradient. Input resistance and local temporal summation is similar across the somatodendritic axis, with I_h making a significant contribution. As in pyramidal neurons, synaptic TS is also normalized across the somatodendritic axis, with I_h a strong component.

Discussion

We have described a principal neuron of the hippocampus with pyramidal morphology, the PLP neuron, that has a reversed somatodendritic gradient of I_h compared to CA1 hippocampal and neocortical pyramidal neurons. PLP neurons lack interneuronal markers and project to both the septum and olfactory bulb, suggesting that they are excitatory principal neurons of the hippocampus. They possess a high somatic I_h density, comparable to that seen in the mid-apical dendrites of CA1 pyramidal neurons, and a relatively low dendritic I_h that declined to a lower density with dendritic distance. While the somatodendritic gradient of I_h was different from pyramidal neurons, I_h voltage-dependent activation and activation time constants were similar in both PLP and pyramidal neurons, suggesting that I_h in both neuron types has a similar composition of HCN subunits.

Prior studies have shown that I_h is present at high density in the dendrites of pyramidal neurons in both CA1 hippocampus and the neocortex (Magee, 1998; Berger *et al.* 2001). The present study demonstrates that this pattern is not a universal feature of neurons with pyramidal morphology. The reversed I_h distribution in PLP neurons compared to CA1 pyramidal neurons is all the more striking considering that the apical dendritic arbors of these two neurons traverse the same hippocampal strata – the stratum radiatum and stratum lacunosum moleculare – and probably receive some of the same excitatory afferent inputs (Maccaferri & McBain, 1996*b*; Gulyas *et al.* 1998). This suggests that h-channel somatodendritic distribution is specific to neuronal type and not simply a function of dendritic morphology or excitatory synaptic input. Of note, a different I_h distribution is seen in cerebellar Purkinje cells in which I_h density is uniform from soma to dendrites (Hausser & Clark, 1997), showing that other patterns may be seen in non-pyramidal neurons.

I_h active at rest decreases the temporal summation of EPSPs by gradually deactivating (producing a net outward current), thus opposing the summated depolarization. In pyramidal neurons, I_h tends to 'normalize' the temporal summation of EPSPs evoked at distal dendritic locations to the value seen at proximal locations, by compensating for the increase in TS that would occur through passive propagation of distal dendritic potentials to the soma (Magee, 1999). In PLP neurons, the same phenomenon appears to occur, with quantitatively similar summation of distally evoked EPSPs compared to summation of EPSP-like voltage transients at the soma. This suggests, as suspected on theoretical grounds, that normalization of temporal summation may occur with a variety of I_h subcellular distribution patterns (Magee, 1999). Unlike in pyramidal neurons, however, local temporal summation in PLP neurons was not different for dendritic *versus* somatic recording sites; this probably reflects the shallower I_h gradient ($\sim$2-fold change *versus* 7-fold in CA1 pyramidal neurons), and the shorter apical dendritic tree found in PLP neurons.

PLP neurons share many characteristics with the previously described radiatum giant cells, including somatic size and location, lack of staining for interneuronal markers, and extra-hippocampal axonal projections (Gulyas *et al.* 1998; Kirson & Yaari, 2000; Savic & Sciancalepore, 2001). In light of these similarities, this study shows that PLPs probably represent a subtype of RGCs. In particular, PLP neurons are probably the 'P-cell-like' variety described by Gulyas *et al.* (1998) which comprises approximately 20% of the RGC population. PLPs probably also share RGC patterns of innervation in area CA1 from stratum radiatum afferents, and presumably make excitatory synapses as has been shown for RGCs on an ultrastructural level (Gulyas *et al.* 1998), although this was not demonstrated in PLP neurons. The typical RGC morphology, however, possesses an inverted pyramidal or shield-shaped soma, with two symmetrical apical dendrites emanating from the apices of the soma (as seen in Fig. 3*B*). The distinct pyramidal morphology of PLPs compared to that of the typical non-pyramidal, bidendritic morphology of RGCs suggests that it is appropriate to distinguish these two types of neurons.

Little is known about the ion channel distributions in typical RGCs, but study of h-channels and other ion channel types in these cells may be useful in understanding how the excitability of these neurons differs from PLPs.

The function of PLPs and RGCs is similarly unknown. That they appear to project more strongly to the olfactory bulb than CA1 hippocampal pyramidal neurons suggests they may subserve a different functional role in the hippocampus. On a more basic level, however, we believe that PLP neurons will be a useful model system for understanding how I_h affects signal integration in pyramidal neurons, given its reversed somatodendritic I_h distribution compared to CA1 pyramidal neurons. Further, I_h in PLP neurons appears to have almost identical biophysical properties to that in CA1 hippocampal pyramidal neurons, and its somatic location in PLP neurons makes patch-clamp recording far more accessible than the comparable dendritic location in CA1 pyramidal neurons. Thus PLP neurons supply an ideal model system for studying pharmacology and modulation of h-channels (Poolos *et al.* 2006). These considerations underlie our hope that PLPs will emerge as a novel principal neuron of the hippocampus worthy of further investigation.

References

Berger T, Larkum ME & Luscher HR (2001). High I(h) channel density in the distal apical dendrite of layer V pyramidal cells increases bidirectional attenuation of EPSPs. *J Neurophysiol* **85**, 855–868.

Bullis JB, Jones TJ & Poolos NP (2004). H-channel distribution in pyramidal-like principal neurons in stratum radiatum of hippocampus differs from pyramidal neurons. *Soc Neurosci Abs* **29**.

Chen S, Wang J & Siegelbaum SA (2001). Properties of hyperpolarization-activated pacemaker current defined by coassembly of HCN1 and HCN2 subunits and basal modulation by cyclic nucleotide. *J Gen Physiol* **117**, 491–504.

Christie BR, Franks KM, Seamans JK, Saga K & Sejnowski TJ (2000). Synaptic plasticity in morphologically identified CA1 stratum radiatum interneurons and giant projection cells. *Hippocampus* **10**, 673–683.

Colbert CM, Magee JC, Hoffman DA & Johnston D (1997). Slow recovery from inactivation of Na^+ channels underlies the activity-dependent attenuation of dendritic action potentials in hippocampal CA1 pyramidal neurons. *J Neurosci* **17**, 6512–6521.

Day M, Carr DB, Ulrich S, Ilijic E, Tkatch T & Surmeier DJ (2005). Dendritic excitability of mouse frontal cortex pyramidal neurons is shaped by the interaction among HCN, Kir2, and Kleak channels. *J Neurosci* **25**, 8776–8787.

Dickson CT, Magistretti J, Shalinsky MH, Fransen E, Hasselmo ME & Alonso A (2000). Properties and role of I(h) in the pacing of subthreshold oscillations in entorhinal cortex layer II neurons. *J Neurophysiol* **83**, 2562–2579.

Fiala JC & Harris KM (1999). Dendrite structure. In *Dendrites*, ed. Stuart G, Spruston N & Häusser M, pp. 1–34. Oxford University Press, Oxford, New York.

Freund TF & Buzsaki G (1996). Interneurons of the hippocampus. *Hippocampus* **6**, 347–470.

Gulyas AI, Hajos N & Freund TF (1996). Interneurons containing calretinin are specialized to control other interneurons in the rat hippocampus. *J Neurosci* **16**, 3397–3411.

Gulyas AI, Toth K, McBain CJ & Freund TF (1998). Stratum radiatum giant cells: a type of principal cell in the rat hippocampus. *Eur J Neurosci* **10**, 3813–3822.

Harris NC & Constanti A (1995). Mechanism of block by ZD 7288 of the hyperpolarization-activated inward rectifying current in guinea pig substantia nigra neurons in vitro. *J Neurophysiol* **74**, 2366–2378.

Hausser M & Clark BA (1997). Tonic synaptic inhibition modulates neuronal output pattern and spatiotemporal synaptic integration. *Neuron* **19**, 665–678.

Hausser M & Mel B (2003). Dendrites: bug or feature? *Curr Opin Neurobiol* **13**, 372–383.

Hausser M, Spruston N & Stuart GJ (2000). Diversity and dynamics of dendritic signaling. *Science* **290**, 739–744.

Hsu M & Buzsaki G (1993). Vulnerability of mossy fiber targets in the rat hippocampus to forebrain ischemia. *J Neurosci* **13**, 3964–3979.

Johnston D, Magee JC, Colbert CM & Cristie BR (1996). Active properties of neuronal dendrites. *Annu Rev Neurosci* **19**, 165–186.

Jung HY, Mickus T & Spruston N (1997). Prolonged sodium channel inactivation contributes to dendritic action potential attenuation in hippocampal pyramidal neurons. *J Neurosci* **17**, 6639–6646.

Kanai Y, Bhide PG, DiFiglia M & Hediger MA (1995). Neuronal high-affinity glutamate transport in the rat central nervous system. *Neuroreport* **6**, 2357–2362.

Kirson ED & Yaari Y (2000). Unique properties of NMDA receptors enhance synaptic excitation of radiatum giant cells in rat hippocampus. *J Neurosci* **20**, 4844–4854.

Lupica CR, Bell JA, Hoffman AF & Watson PL (2001). Contribution of the hyperpolarization-activated current (I(h) to membrane potential and GABA release in hippocampal interneurons. *J Neurophysiol* **86**, 261–268.

Maccaferri G & McBain CJ (1996*a*). The hyperpolarization-activated current (I_h) and its contribution to pacemaker activity in rat CA1 hippocampal stratum oriens-alveus interneurones. *J Physiol* **497**, 119–130.

Maccaferri G & McBain CJ (1996*b*). Long-term potentiation in distinct subtypes of hippocampal nonpyramidal neurons. *J Neurosci* **16**, 5334–5343.

Magee JC (1998). Dendritic hyperpolarization-activated currents modify the integrative properties of hippocampal CA1 pyramidal neurons. *J Neurosci* **18**, 7613–7624.

Magee JC (1999). Dendritic I_h normalizes temporal summation in hippocampal CA1 neurons. *Nat Neurosci* **2**, 508–514.

McBain CJ & Fisahn A (2001). Interneurons unbound. *Nat Rev Neurosci* **2**, 11–23.

McCormick DA & Pape HC (1990). Properties of a hyperpolarization-activated cation current and its role in rhythmic oscillation in thalamic relay neurones. *J Physiol* **431**, 291–318.

Nolan MF, Malleret G, Dudman JT, Buhl DL, Santoro B, Gibbs E, Vronskaya S, Buzsaki G, Siegelbaum SA, Kandel ER & Morozov A (2004). A behavioral role for dendritic integration: HCN1 channels constrain spatial memory and plasticity at inputs to distal dendrites of CA1 pyramidal neurons. *Cell* **119**, 719–732.

Paxinos G & Watson C (1998). *The Rat Brain in Stereotaxic Coordinates*. Academic Press, San Diego.

Poolos NP, Bullis JB & Roth MK (2006). Modulation of h-channels in hippocampal pyramidal neurons by p38 mitogen-activated protein kinase. *J Neurosci* **26**, 7995–8003.

Poolos NP, Migliore M & Johnston D (2002). Pharmacological upregulation of h-channels reduces the excitability of pyramidal neuron dendrites. *Nat Neurosci* **5**, 767–774.

Rall W (1959). Branching dendritic trees and motoneuron membrane resistivity. *Exp Neurol* **1**, 491–527.

Rall W (1962). Electrophysiology of a dendritic neuron model. *Biophys J* **2**, 145–167.

Reyes A (2001). Influence of dendritic conductances on the input–output properties of neurons. *Annu Rev Neurosci* **24**, 653–675.

Robinson RB & Siegelbaum SA (2003). Hyperpolarization-activated cation currents: from molecules to physiological function. *Annu Rev Physiol* **65**, 453–480.

Rothstein JD, Martin L, Levey AI, Dykes-Hoberg M, Jin L, Wu D, Nash N & Kuncl RW (1994). Localization of neuronal and glial glutamate transporters. *Neuron* **13**, 713–725.

Sakmann B & Neher E (1995). *Single-channel Recording*. Plenum Press, New York.

Santoro B, Chen S, Luthi A, Pavlidis P, Shumyatsky GP, Tibbs GR & Siegelbaum SA (2000). Molecular and functional heterogeneity of hyperpolarization-activated pacemaker channels in the mouse CNS. *J Neurosci* **20**, 5264–5275.

Savic N & Sciancalepore M (2001). Electrophysiological characterization of 'giant' cells in stratum radiatum of the CA3 hippocampal region. *J Neurophysiol* **85**, 1998–2007.

Segev I & London M (2000). Untangling dendrites with quantitative models. *Science* **290**, 744–750.

Stuart GJ & Sakmann B (1994). Active propagation of somatic action potentials into neocortical pyramidal cell dendrites. *Nature* **367**, 69–72.

Stuart G & Spruston N (1998). Determinants of voltage attenuation in neocortical pyramidal neuron dendrites. *J Neurosci* **18**, 3501–3510.

Ulens C & Tytgat J (2001). Functional heteromerization of HCN1 and HCN2 pacemaker channels. *J Biol Chem* **276**, 6069–6072.

van Groen T & Wyss JM (1990). Extrinsic projections from area CA1 of the rat hippocampus: olfactory, cortical, subcortical, and bilateral hippocampal formation projections. *J Comp Neurol* **302**, 515–528.

Velumian AA, Zhang L, Pennefather P & Carlen PL (1997). Reversible inhibition of I_K, I_{AHP}, I_h and I_{Ca} currents by internally applied gluconate in rat hippocampal pyramidal neurones. *Pflugers Arch* **433**, 343–350.

Vetter P, Roth A & Hausser M (2001). Propagation of action potentials in dendrites depends on dendritic morphology. *J Neurophysiol* **85**, 926–937.

Williams SR, Christensen SR, Stuart GJ & Hausser M (2002). Membrane potential bistability is controlled by the hyperpolarization-activated current I_H in rat cerebellar Purkinje neurons in vitro. *J Physiol* **539**, 469–483.

Williams SR & Stuart GJ (2000). Site independence of EPSP time course is mediated by dendritic I_h in neocortical pyramidal neurons. *J Neurophysiol* **83**, 3177–3182.

Acknowledgements

This work was supported by NIH NINDS (NP) and the Epilepsy Foundation (JB).